J Appl Electrochem (2009) 39:653–661
DOI 10.1007/s10800-008-9705-1

ORIGINAL PAPER

Electrochemical polymerization and characterization of a poly(azulene)-TiO_2 nanoparticle composite film

R.-M. Latonen · B. Meana Esteban · C. Kvarnström · A. Ivaska

Received: 12 February 2008 / Accepted: 22 October 2008 / Published online: 12 November 2008

Abstract A poly(azulene)-TiO_2 composite film (PAz-TiO_2) was synthesized electrochemically by oxidation of azulene in an electrolyte medium containing TiO_2 nanoparticles. Polymerization was performed under magnetic stirring in an acetonitrile solution containing tetrabutylammonium hexafluorophosphate as the electrolyte salt. Influence of the concentration of TiO_2 in the reaction suspension on the electrochemical and optical properties and on the structure of the composite films was studied by cyclic voltammetry, ex situ Raman and FTIR reflection spectroscopy and in situ UV–vis and FTIR spectroelectrochemical techniques. Morphology of the composite films was studied by Scanning Electron Microscopy and the amount and distribution of the TiO_2 nanoparticles within the polymeric matrix by Inductively Coupled Plasma Mass Spectrometry with laser ablation. Addition of TiO_2 in the reaction suspension had a small catalytic activity for the polymerization of Az. Inclusion of TiO_2 nanoparticles in PAz did not affect the voltammetric behavior or the chemical structure of the formed polymer films. However, a different chain conformation and morphology of the film was formed when synthesized in presence of TiO_2 compared to the plain PAz film. It was also found that the film morphology was more homogeneous when the concentration of TiO_2 was $\geq$10 mM in the polymerization solution than films polymerized without any TiO_2.

R.-M. Latonen (✉) · B. Meana Esteban · C. Kvarnström · A. Ivaska
Process Chemistry Centre, c/o Laboratory of Analytical Chemistry, Åbo Akademi University, Biskopsgatan 8, 20500 Turku/Åbo, Finland
e-mail: rlatonen@abo.fi

Keywords Poly(azulene) · TiO_2 · Composite · Electropolymerization · In situ spectroelectrochemistry

1 Introduction

There is an increasing demand for environmentally clean and renewable alternative energy sources. Silicon based photovoltaic (PV) cells for capturing the available energy from sunlight and turning it into electric power lack flexibility, are heavy and have high material and production costs which limit their applicability. Therefore, the inorganic mesoporous semiconductor TiO_2 has been introduced as an effective electron-acceptor material together with a sensitizing dye as an electron-donor material in the concept of the Grätzel cell [1]. There are also some drawbacks in dye-sensitized PV cells like evaporation of electrolyte, stability of the electrolyte and the dye, together with high cost and limited availability of the dye [2]. Development of PV cells based on nanocrystalline inorganic materials, like TiO_2, and organic electronic materials, such as conducting polymers (CP), has become a subject of increasing interest [3–8]. The high ability to absorb light in the visible part of the spectrum, the high mobility of the charge carriers and the low cost, easy availability and flexibility of CPs make them good candidates for applications in PV cells.

Azulene (Az) is a non-benzenoid aromatic hydrocarbon and oxidation converts it to a resonance-stabilized azulenylium carbocation. The cation is more stable than azulene itself and has an electron-donating feature due to the partial negative charge of the five membered ring and the partial positive charge of the seven membered ring of the monomer, which influences also electropolymerization [9]. Scheme 1 shows redox reaction of poly(azulene) (PAz) and distribution of charge in the monomer units. It has been

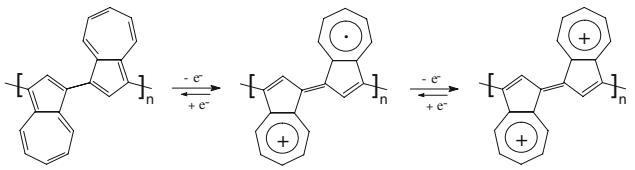

Scheme 1 Oxidation of PAz leading to radical cation (polaron) and dication (bipolaron)

reported that 1-carboxyazulene in its excited state can inject an electron into the conduction band of TiO_2 within the fs time scale [10]. This unique electron-donating property can be utilized in solar cell applications. Furthermore, the easy electropolymerization process of Az [11, 12] having a relatively low oxidation potential, gives a planar structure to PAz in its conducting form. This results in a rather high electrical conductivity and broad absorbance in the UV and visible wavelength ranges and makes PAz to an attractive material for PV cells.

The diffusion length of excitons in CPs is typically 5–15 nm and to get a well-defined interface between the acceptor-type material and the donor-type CP to prevent unwanted recombination is a demanding task. Different CP-TiO_2 composite materials have been prepared both by chemical [13–15] and electrochemical [16–21] means. These composite materials have been synthesized for different applications: electrochemical actuators [17], corrosion protection [18] and PV cells [13, 19, 21]. In this study a PAz-TiO_2 composite has been synthesized by electrochemical polymerization of Az in a suspension containing TiO_2 nanoparticles. The composite films have been characterized by cyclic voltammetry (CV), in situ UV–vis and FTIR spectroelectrochemistry, ex situ FTIR and Raman spectroscopy, Scanning Electron Microscopy (SEM) and Inductively Coupled Plasma Mass Spectrometry with laser ablation (LA ICP-MS).

2 Experimental

Polymerization of the studied films and the charging–discharging experiments were carried out in a conventional three-electrode one-compartment electrochemical cell. The cell was connected to an Autolab PGSTAT100 potentiostat using General Purpose Electrochemical System (GPES) software. The working electrode was either a Pt-disk ($A = 0.07\ cm^2$) sealed in a Teflon® body or an optically transparent indium tin oxide (ITO) glass (Delta Technologies, Limited, 4–8 Ω/square). The Pt-disk electrode was polished mechanically with 0.03 μm alumina powder before each polymerization and the ITO substrates were washed with chloroform and acetone during 30 min in an ultrasonic bath. A Pt wire was used as the counter electrode. The poly(azulene) (PAz) and poly(azulene)-TiO_2 composite films were polymerized by potential cycling between −0.6 V and 1.2 V with a scan rate of 50 mV s^{-1} in 0.1 M tetrabutylammonium hexafluorophosphate ($TBABF_6$, Fluka) electrolyte salt dissolved in acetonitrile (ACN, Lab-Scan). All potential values are measured against a Ag wire covered with AgCl pseudo reference electrode (calibrated against ferrocene/ferrocenium, $E_{redox} = 0.36$ V in 0.1 M $TBAPF_6$-ACN). ACN was stored over CaH_2 and freshly distilled and dried over basic alumina (≈150 mesh, Aldrich) before use. The electrolyte salt $TBAPF_6$ was dried at 80°C under vacuum for 1 h. Concentration of the monomer azulene (Az, Aldrich) was 10 mM and it was used as received. Different concentrations of TiO_2 (Degussa, Aeroxide P25, average particle size 21 nm) in the polymerization suspension were studied (2, 4, 10, 20 and 50 mM). After adding the nanoparticle TiO_2 powder into the electrolyte solution it was let to disperse by ultrasonication for 30 min. TiO_2 was used without further treatment and the polymerization was performed under magnetic stirring. All solutions were deaerated with nitrogen prior to measurements and all the measurements were done under nitrogen atmosphere.

In the ex situ FTIR reflection and Raman measurements of the PAz and PAz-TiO_2 composite films the polymers were deposited on ITO glass substrates. 22 scans were used for polymerization and the films were rigorously washed with pure ACN after synthesis. The FTIR measurements were performed using a Seagull™ variable angle reflectance accessory (Harric Scientific) with an angle of incidence of 60° and 500 interferograms with a resolution of 4 cm^{-1} were recorded for each spectrum. The spectra were recorded on a Bruker IFS 66/S FTIR instrument equipped with an MCT detector. The Raman spectra were recorded on a Renishaw Ramascope (system 100) equipped with a Leica DMLM microscope and connected to a CCD camera. Si with a Raman peak at 520 cm^{-1} was used for calibration of the wavenumber scale. The excitation wavelengths (λ_{exc}) of the lasers used were 514, 633 and 780 nm.

For the in situ FTIR-ATR studies the PAz and PAz-TiO_2 composite films were synthesized on a ZnSe reflection element (size 10 × 10 × 2 mm) covered with a thin layer of Pt (≈20 nm) which served as the working electrode. This reflection element was attached to the spectroelectrochemical cell made of Teflon® and constructed as a flow cell. Construction details have been described earlier [22]. The reference electrode was the same as in the CV experiments and a Pt plate was used as the counter electrode. A beam condenser 4XF-BR3 (Harrick Scientific) served as the attachment to the FTIR spectrometer. The doping process of the polymer films was studied in a monomer-free electrolyte solution by recording FTIR

spectra in situ during a slow voltammetric scan (5 mV s^{-1}) between −0.4 and 1.1 V. For each spectrum 32 interferograms were co-added and spectral resolution was 4 cm^{-1}. The measured spectra were related to a reference spectrum taken prior to the studied oxidation reaction. The spectra shown in this work describe therefore the spectral differences from the reference state. The same FTIR instrument as in the ex situ reflection measurements was used.

For the in situ UV–vis spectroscopic experiments the PAz and PAz-TiO_2 composite films were formed on ITO glass substrates in the same way as described earlier using 10 scans instead of 22. The path length of the quartz cuvette used was 1 cm. The reference electrode was the same as in the CV experiments and a Pt wire was used as the counter electrode. The potential was held at a constant value for 80 s before each measurement and increased then by steps of 200 mV in the beginning of the positive potential scan and by steps of 100 mV at the potential range where the Faradaic process occurs. The spectra were recorded between 340 and 1,100 nm on a Hitachi U-2001 spectrophotometer.

A Zeiss, Leo 1530 Gemini Scanning Electron Microscope with a ThermoNoran, Vantage X-ray detector was used to obtain the SEM micrographs. The used acceleration voltage was 3.7 kV for the PAz film and the PAz-TiO_2 film made with 2 mM TiO_2 in the polymerization suspension and 15 kV for the PAz-TiO_2 film made with 10 mM TiO_2. The LA ICP-MS spectra were recorded on a Perkin Elmer Elan 6100 DRC Plus masspectrometer. The New Wave Research UP-213 Laser Ablation System (laser wavelength 213 nm, beam diameter 25 μm) was used to scan the laser over a 3.6 mm long line with a rate of 20 μm s^{-1}.

3 Results and discussion

3.1 Polymerization and cyclic voltammetric characterization of the PAz-TiO_2 composite films

During the 25 potential cycles in the monomer solution a continuous growth of the polymer film both with and without TiO_2 was observed. The first cycles in the CVs showing the polymerization of Az and polymerization of Az in a suspension containing 2 mM TiO_2 in $TBAPF_6$-ACN are shown in Fig. 1a. It can be observed that oxidation of Az starts at a slightly lower potential (≈0.4 V) in presence of TiO_2 compared to polymerization of Az without any TiO_2 (≈0.5 V). An even more significant difference can be observed in the increase in the oxidation current. It increases more steeply after the onset potential within the potential scan in the presence of TiO_2. The same kind of results was also observed with other TiO_2 concentrations and on both Pt and ITO substrates. An increase in the concentration of TiO_2 (above 2 mM) did not, however, have any influence on the onset potential. It can be concluded that the presence of TiO_2 demonstrates the catalytic activity of TiO_2 for the polymerization of Az. Therefore, already at lower anodic potential a monomer oxidation can be observed. This may be due to the electron withdrawing effect of TiO_2 that accelerates oxidation of the monomer. Overoxidation of the formed film and unwanted side reactions competing with film formation are also avoided when a lower onset potential for polymerization is used. The same kind of effect of TiO_2 nanoparticles has also been observed on electropolymerization of pyrrole [16].

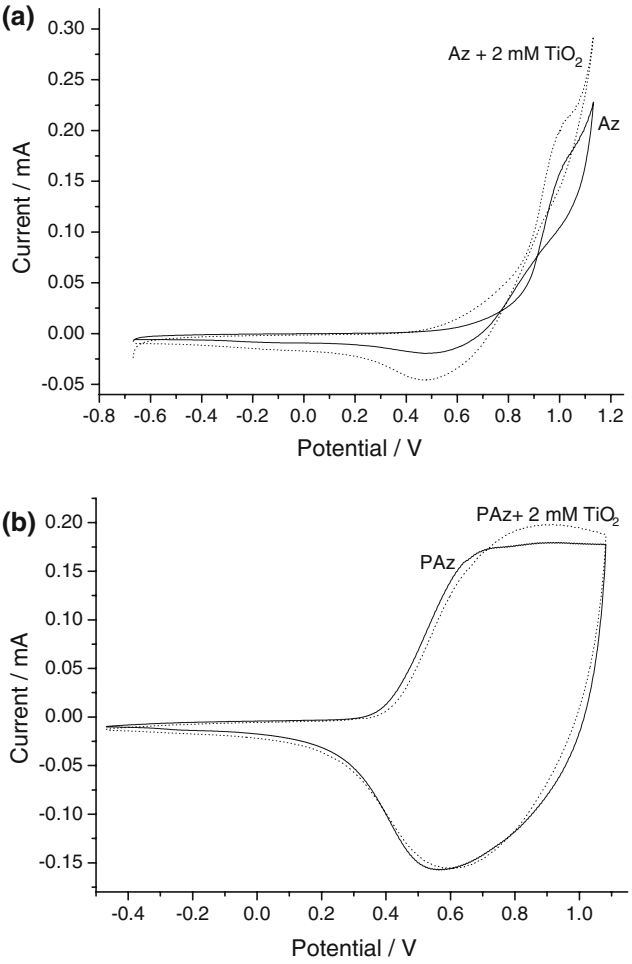

Fig. 1 **a** The first cycles in polymerization of 10 mM Az (solid line) and 10 mM Az with 2 mM TiO_2 (dotted line) in $TBAPF_6$-ACN electrolyte solution. Scan rate 50 mV s^{-1}. **b** The cyclic voltammograms (the 3rd scan) of PAz (solid line) and PAz-TiO_2 composite films (2 mM TiO_2, dotted line) in 0.1 M $TBAPF_6$-ACN monomer-free electrolyte solution (25 cycles used during polymerization). Scan rate 20 mV s^{-1}

The charging–discharging reactions of PAz and PAz-TiO_2 composite films were studied in monomer-free electrolyte solutions. The CV responses of the PAz and PAz-TiO_2 composite films made as in Fig. 1a are shown in

Fig. 1b. The films were made with 25 potential cycles (total amount of charge consumed during polymerization of Az was 143 mC and during polymerization of Az + 2 mM TiO_2 was 169 mC). The charge involved in the charging–discharging reaction and the oxidation and reduction peak potentials are almost the same in all the films made with different concentrations of TiO_2 (2, 4, 10, 20, 50 mM).

3.2 FTIR characterization

The ex situ FTIR spectra of PAz films synthesized with and without TiO_2 in $TBAPF_6$-ACN electrolyte solution on ITO glass are shown in Fig. 2. The spectrum of PAz is compared with the spectrum of PAz-TiO_2 composite film polymerized in a 0.1 M $TBAPF_6$-ACN electrolyte solution having 4 mM TiO_2. The FTIR spectra show that inclusion of TiO_2 into PAz films do not have any influence on the chemical structure of PAz which conforms that the PAz-TiO_2 composite film has the same characteristic chemical structure as PAz. The peaks at 1,565 cm^{-1} [23, Table 11.1, Table 11.2, Table 11.4, Table 22.1, p. 278], [24, Table 9.22, Table 9.23], [25, 26], at 1,475 cm^{-1} [23, Table 11.1] and at 1,394 cm^{-1} [25, 26] in both spectra are assigned to aromatic C=C ring stretching vibrations. The =C–H ring out-of-plane deformation vibration can be seen as a strong band at 739 cm^{-1} [23, Table 11.2], [24, Table 9.22], [25, 26] and as a couple of weak bands at 875 and 944 cm^{-1} [24, Table 9.22]. A combination and overtone of the same =C–H ring out-of-plane hydrogen deformation can be seen as a weak band at around 1,690 cm^{-1} [24, Table 9.23]. The vibrational bands in the wavenumber region 1,020–1,290 cm^{-1} can be assigned to =C–H in-plane deformation vibrations [23, Table 11.4]. The strong band at 839 cm^{-1} in both spectra is due to the vibration originating from the doping anion PF_6^- [23, Table 22.1]. Any bands characteristic for TiO_2 in the wavenumber regions 700–660 cm^{-1} and 525–460 cm^{-1} [23, p. 278] could not be found in the recorded spectra. This was also the case in the FTIR spectrum of polypyrrole-TiO_2 composite film electrochemically synthesized on mild steel [27].

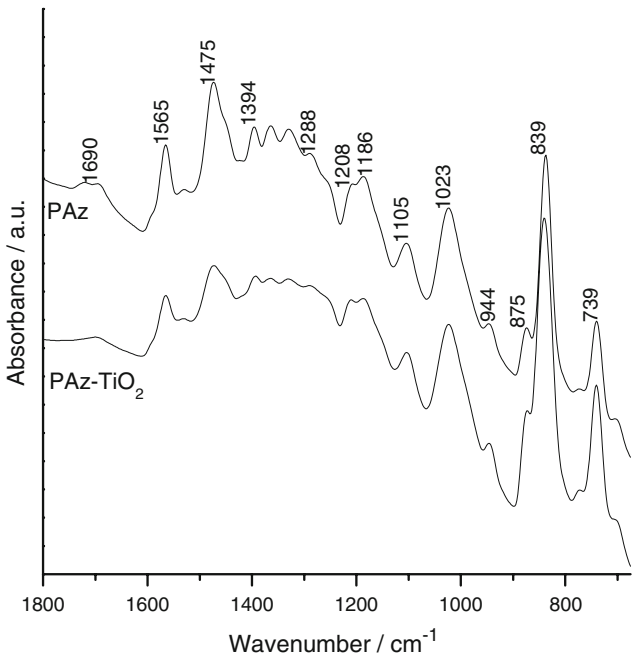

Fig. 2 Ex situ FTIR spectra of PAz and PAz-TiO_2 composite (4 mM TiO_2) made in 0.1 M $TBAPF_6$-ACN

The p-doping process, i.e. oxidation of the film by increasing the electrode potential, of both PAz and PAz-TiO_2 composite (10 mM TiO_2 in polymerization solution) films was studied by in situ FTIR-ATR spectroscopy in a spectroelectrochemical cell described earlier [22]. The spectra of PAz-TiO_2 composite film recorded in 0.1 M $TBAPF_6$-ACN electrolyte solution during p-doping process are shown in Fig. 3a. The CV is shown in the inset of Fig. 3a. The arrows indicate at which potential the different spectra have been measured. The spectra are dominated by the electronic absorption at high energy. The electronic absorption continuously increases and shifts to lower wavenumber region, i.e. lower energy upon p-doping of the film. Two absorbance maxima (spectra 8–12), one at approximately 3,000 cm^{-1} and the other at 4,800 cm^{-1}, can be observed. Enlargement of the spectra in the wavenumber region 1,700–700 cm^{-1} is shown in Fig. 3b. It shows the so-called infrared active vibration (IRAV) bands, which grow during p-doping process due to positive charges inserted in the polymer chain resulting in changes in the dipole moment giving rise to new vibrations. The pattern of the IRAV bands of PAz-TiO_2 composite film is complex and the positions of the main peaks are indicated in Fig. 3b. The changes in the spectra are more pronounced until approximately 800 mV (spectrum 9) is reached where the maximum doping level of the film can be assumed to be achieved. The changes in the absorbance are highly reversible upon reduction of the film and the absorbance decreases until it reaches its initial value. A comparison of the spectra of pure PAz and PAz-TiO_2 composite films measured at 1.0 V during p-doping is shown in Fig. 4a. It can be observed that the electronic absorption of the PAz-TiO_2 composite film starts at a wavenumber that is approximately 300 cm^{-1} lower compared with the spectrum of PAz. The two maxima of this absorption (in both spectra) are also shifted to lower energy in the film containing TiO_2 (from 3,700 to 3,000 cm^{-1} and from 6,200 to 4,800 cm^{-1}). The differences might originate from different chain conformation and morphology of the synthesized films. The TiO_2 nanoparticles have also the property of

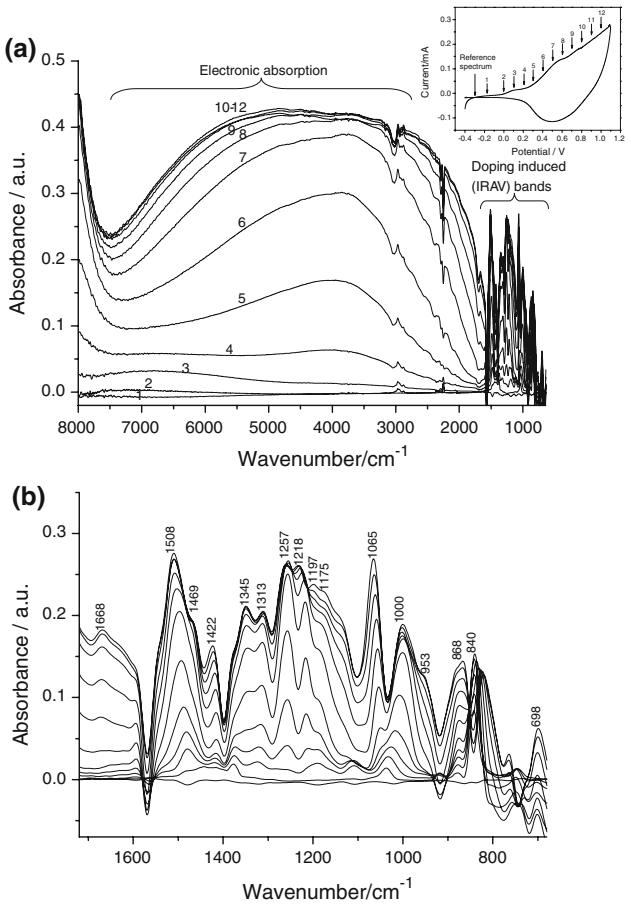

Fig. 3 In situ FTIR-ATR difference spectra recorded during oxidation of PAz-TiO_2 nanocomposite film (10 mM TiO_2) in 0.1 M $TBAPF_6$-ACN electrolyte solution (**a**) in the wavenumber region 8,000–700 cm^{-1} (the numbers indicate the potential values where each spectrum was recorded and refer to the cyclic voltammogram in the inset). **b** Enlargement of the spectra in the wavenumber region 1,700–700 cm^{-1}

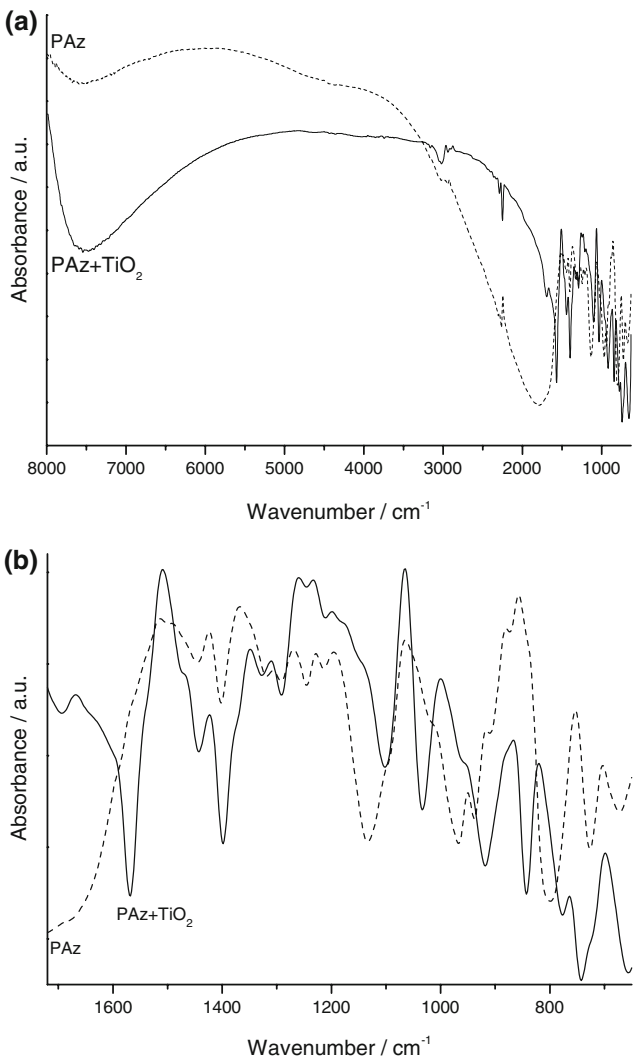

Fig. 4 Comparison of in situ FTIR-ATR difference spectra of pure PAz and PAz-TiO_2 composite film (10 mM TiO_2) measured at 1.0 V during p-doping in 0.1 M $TBAPF_6$-ACN electrolyte solution, (**a**) wavenumber region 8,000–700 cm^{-1} and (**b**) wavenumber region 1,700–700 cm^{-1}

accepting the electrons released during doping which also can result in a shift of the position of the electronic absorption towards lower energy. A comparison of the IRAV bands between the PAz and PAz-TiO_2 films is shown in Fig. 4b. The same shape of both spectra in this wavenumber region confirms that they are from the same kind of material.

3.3 In situ UV-visible spectroelectrochemical characterization

In the UV–vis spectroelectrochemical measurements the p-doping process of both PAz and PAz-TiO_2 composite (10 mM TiO_2 in polymerization solution) films were studied by recording spectra at different potentials applied to the film. Before recording the spectra the film was held at each potential for 80 s in order to reach a stable current response. The polymers were synthesized by potential cycling in 0.1 M $TBAPF_6$-ACN electrolyte solution on ITO glass electrodes under magnetic stirring. The in situ UV–vis spectra of stepwise doping of the PAz and PAz-TiO_2 composite films are shown in Fig. 5a, b, respectively. The valence to conduction band (π–π^*), transition, which is connected to the mean conjugation length of the chains and to the delocalization of the π electrons [28], is seen in the spectrum of neutral PAz at 412 nm and in the spectrum of neutral PAz-TiO_2 composite at 434 nm. Due to the absorption maximum of the composite film located at higher wavelength it can be concluded that inclusion of TiO_2 nanoparticles into the PAz film rather increases than decreases delocalization of the π electrons. The chain conformation is probably different in the PAz-TiO_2 film from the PAz film. The width of the energy gap between

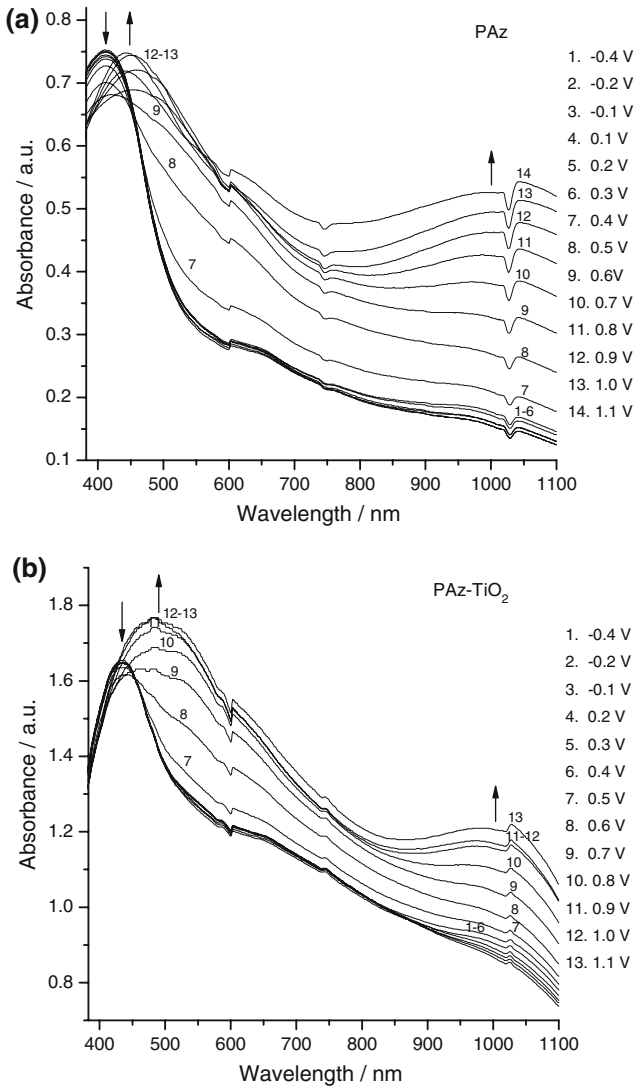

Fig. 5 The in situ UV-vis spectra of stepwise doping of (**a**) PAz, and (**b**) PAz-TiO_2 composite films (10 mM TiO_2 in polymerization solution) in 0.1 M $TBAPF_6$-ACN electrolyte solution

the valence and conduction bands of PAz-TiO_2 composite was smaller than in PAz. The energy gap was determined from the onsets of the π–π^* transition bands recorded in the neutral forms of the polymers. The bandgap value of PAz was estimated to 2.2 eV and that of the PAz-TiO_2 composite to 1.9 eV. In our experiment the composite film was thicker than the pure PAz film which also has an influence on the location of the absorption maximum. In the case of the composite film a part of the shift of the π–π^* transition to lower energy may depend on the film thickness. It can, however, be said that inclusion of TiO_2 into the PAz films do not affect the structure of the polymer in a negative way. The same results were also obtained by the FTIR measurements as discussed earlier. Electrochemical doping of the films results in slight bleaching of the π–π^* transition with a simultaneous growth of two new absorption bands at higher wavelength due to continuous change of the film into conducting form [28]. At the beginning of the p-doping process, i.e. at potentials higher than 0.4 V, absorption bands at around 446 nm and at 1,000 nm for PAz and at 487 nm and at 1,000 nm for PAz-TiO_2 composite film start to grow in the spectra. These new doping induced bands (at 446 nm and at 487 nm) are located at only 34 nm in the case of PAz and 53 nm in the case of PAz-TiO_2 composite towards lower energy with respect to the π–π^* transition. These doping induced absorption bands are presistant and do not vanish even during further increase of the potential which is often the case with many other conducting polymer films. These results show that PAz and also PAz-TiO_2 composite films are materials with broad absorbance in the UV–vis spectral region, which is a benefit in the further development of these materials for solar cell applications.

3.4 Raman characterization

Figure 6 shows the Raman spectrum of the PAz film synthesized in a suspension with 10 mM TiO_2 in $TBAPF_6$-ACN compared to the spectrum of PAz and the spectrum of pure TiO_2. The spectra were measured with three different laser excitation wavelengths (λ_{exc}) (514 nm, Fig. 6a, 633 nm, Fig. 6b and 780 nm, not shown). Due to high fluorescence in the spectra measured with $\lambda_{exc} = 780$ nm the possible peaks originating from TiO_2 could not be seen. The two broad bands at 1,583 cm^{-1} and at around 1,360 cm^{-1} in the Raman spectra of both PAz and PAz-TiO_2 composite films measured with $\lambda_{exc} = 514$ nm can be correlated with the so-called G and D bands of disordered graphite, respectively [29]. Raman intensities related to the G band are mainly due to CCC bending vibrations and intensities related to the D band are essentially due to CC stretching contributions [30]. The corresponding bands can be seen at 1,539 cm^{-1} and at 1,321 cm^{-1} in the Raman spectra of the PAz and the PAz-TiO_2 films measured with $\lambda_{exc} = 633$ nm. These bands are shifted with approximately 40 cm^{-1} towards lower energy. The reason is that the vibrations originating from quinoid and neutral units will be differently resonance enhanced by the applied excitation lines. Excitation with $\lambda_{exc} = 514$ nm enhances the resonance effect of the Raman lines originating from the neutral segments of the film, while excitation with $\lambda_{exc} = 633$ nm enhances more the vibrations associated with the quinoid units in the film [31]. It has also been shown that the D band shifts towards lower active frequencies with decreasing energy of the exciting laser line [29]. The Raman spectra of the PAz-TiO_2 nanoparticle composite film studied show clear signs of inclusion of TiO_2 into the films. The Raman-fundamentals in the vibrational spectrum of TiO_2 can be found at 633, 513 and 395 cm^{-1} when $\lambda_{exc} = 514$ nm is used (Fig. 6a) and at

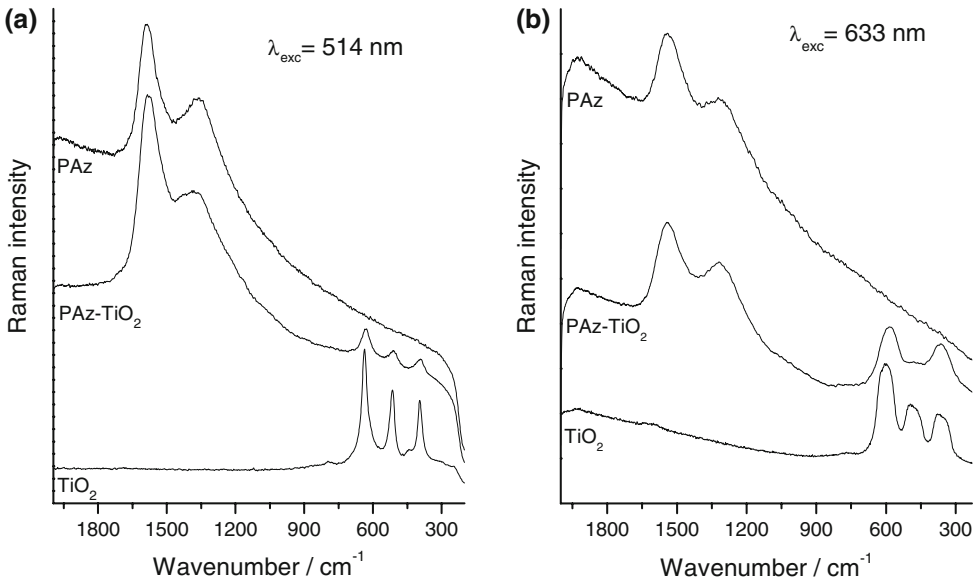

Fig. 6 Raman spectra of PAz (upper spectrum), PAz-TiO_2 composite (10 mM TiO_2, middle spectrum) and pure TiO_2 (undermost spectrum) measured with (**a**) 514 nm laser line and (**b**) 633 nm laser line

585, 472 and 357 cm^{-1} when $\lambda_{exc} = 633$ nm is used (Fig. 6b). Vibrational bands at approximately the same wavenumbers can also be observed in the spectra of anatase crystal structure of TiO_2 at ambient conditions when $\lambda_{exc} = 514$ nm [32] and $\lambda_{exc} = 1{,}064$ nm [33] are used.

3.5 Scanning electron microscopy characterization

Morphologies of the PAz-TiO_2 composite films were studied by SEM and compared with the morphology of the PAz film. Morphologies of the resulted films varied depending on the amount of TiO_2 added to the reaction mixture. The SEM pictures of films synthesized in a suspension containing 2 and 10 mM TiO_2 in $TBAPF_6$-ACN are shown as examples in Fig. 7. The inclusion of TiO_2 nanoparticles ($\varnothing \approx 21$ nm) into PAz films can be seen as a decrease in the grain size with increasing amount of TiO_2 in the reaction suspension. The film also becomes more homogeneous when the amount of TiO_2 in the reaction suspension is increased. High amount of TiO_2 (20 and 50 mM) in the reaction suspension, however, created smaller clusters of TiO_2 which are more frequently located

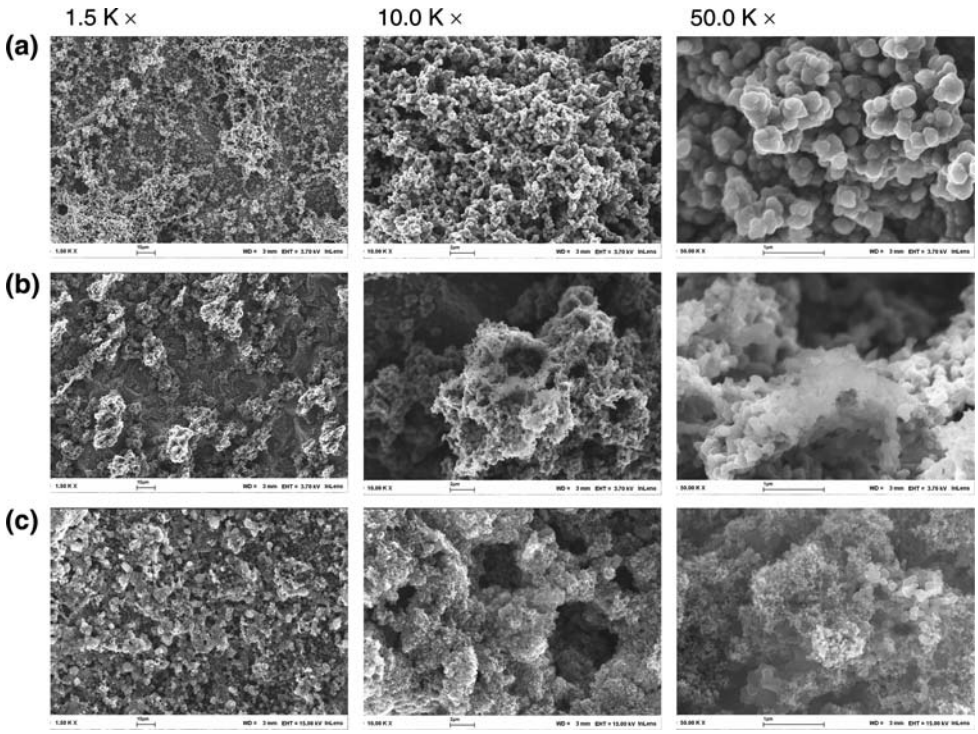

Fig. 7 SEM micrographs of (**a**) PAz and (**b**) and (**c**) PAz-TiO_2 composites synthesized in $TBAPF_6$-ACN (2 mM TiO_2 (**b**) 10 mM TiO_2 (**c**)) with three magnifications (1.5 K×, 10.0 K×, 50.0 K×)

Table 1 Mean intensities of Ti in the different PAz-TiO_2 composite films and their RSD values measured by LA ICP-MS

[TiO_2] (mM)	Mean intensity of Ti (ppm)	RSD (%)
2	2,250	125
4	33,700	50
10	38,800	81
20	7,880	69
50	29,300	24

The films were synthesized in $TBAPF_6$-ACN electrolyte media

on the surface of the polymer film compared to when 2, 4 and 10 mM of TiO_2 was used (images not shown). The number of grains and the grain size in the TiO_2 clusters also seems to grow when the amount of TiO_2 was 50 mM instead of 20 mM in the reaction suspension.

3.6 Inductively coupled plasma mass spectrometry characterization

LA ICP-MS was also used to study the PAz and PAz-TiO_2 composite films. The amount of Ti in the composite films was measured during the laser scan of a 3.6 mm long line over the sample. The measured mean intensities of Ti in the PAz films synthesized in $TBAPF_6$-ACN electrolyte solution with different amount of TiO_2 with the relative standard deviations (RSD) are shown in Table 1. When the concentration of TiO_2 in the reaction suspension was increased from 2 to 4 mM an over 10-fold increase in the mean intensity of Ti in the PAz-TiO_2 composite films measured by LA ICP-MS was observed. An increase in the TiO_2 concentration >4 mM in the reaction suspension did not further increase the Ti concentrations in the films. The sudden decrease in Ti concentration when 20 mM TiO_2 was used in the reaction suspension can be explained by the change in the morphology of the formed film shown by the SEM micrographs. A more even distribution of Ti in the film was, however, observed when a high concentration of TiO_2 (50 mM) was used.

4 Conclusions

Good quality PAz-TiO_2 nanoparticle composite films were synthesized electrochemically on Pt and ITO electrodes by potential cycling in $TBAPF_6$-ACN electrolyte solution under magnetic stirring. 10 mM TiO_2 in the reaction suspension was found to be an adequate amount to make homogeneous films. The formed composite films have the characteristic chemical structure of PAz. Spectroelectrochemical and SEM experiments revealed different chain conformation and morphology of the synthesized films. As a result a more effective delocalization and easier movement of the π-electrons in the nanocomposite film compared to the pure PAz film was observed. The already low bandgap value 2.2 eV of PAz changed to 1.9 eV in the PAz-TiO_2 film.

Acknowledgements This work is a part of the Åbo Akademi University, Process Chemistry Centre, appointed to a National Centre of Excellence by the Academy of Finland for 2000–2011. The authors thank Lic.tech. Paul Ek for performing the LA ICP-MS analyses and M.Sc. Linus Silvander for taking the SEM micrographs.

References

1. Grätzel M (2001) Nature 414:338
2. Senadeera GKR, Pathirathne WMTC (2004) Curr Sci 87:339
3. Senadeera R, Fukuri N, Saito Y, Kitamura T, Wada Y, Yanagida S (2005) Chem Commun 2259
4. Senadeera GKR, Kitamura T, Wada Y, Yanagida S (2005) Solar Energy Mater Solar cells 88:315
5. Senadeera GKR, Kitamura T, Wada Y, Yanagida S (2006) J Photochem Photobiol A 184:234
6. Liu Y, Scully SR, McGehee MD, Liu J, Luscombe CK, Fréchet JMJ, Shaheen SE, Ginley DS (2006) J Phys Chem B 110:3257
7. Song MY, Kim JK, Kim K-J, Kim DY (2003) Synth Met 137:1387
8. Ravirajan P, Haque SA, Durrant JR, Poplavskyy D, Bradley DDC, Nelson J (2004) J Appl Phys 95:1473
9. Zhang X-H, Li C, Wan W-B, Cheng X-X, Wang X-S, Zhang B-W (2007) J Mater Chem 17:642
10. Pagba C, Zordan G, Galoppini E, Piatniski EL, Hore S, Deshayes K, Piotrowiak P (2004) J Am Chem Soc 126:9888
11. Lete C, Meana Esteban B, Kvarnström C, Razus A, Ivaska A (2007) Electrochim Acta 52:6476
12. Meana Esteban B, Lete C, Kvarnström C, Ivaska A (2006) J Phys B 110:23343
13. Wang W, Ji J-S, Lin Y-J, Rwei S-P (2005) Synth Met 155:677
14. Dey A, De S, De A, De SK (2004) Nanotechnology 15:1277
15. Lee IS, Lee JY, Sung JH, Choi HJ (2005) Synth Met 152:173
16. Liu Y-C, Huang J-M, Tsai C-E, Chuang TC, Wang C-C (2004) Chem Phys Lett 387:155
17. He X, Shi G (2006) Sens Actuators B 115:488
18. Lenz DM, Delamar M, Ferreira CA (2003) J Electroanal Chem 540:35
19. Lin Y-J, Wang L, Chiu W-Y (2006) Thin Solid Films 511–512:199
20. Lenz DM, Ferreira CA, Delamar M (2002) Synth Met 126:179
21. Ilieva M, Ivanov S, Tsakova V (2008) J Appl Electrochem 38:63
22. Latonen R-M, Kvarnström C, Ivaska A (2001) J Electroanal Chem 512:36
23. Socrates G (2001) Infrared and Raman characteristic group frequencies, tables and charts, 3rd edn. John Wiley & Sons, Chichester
24. Nyquist RA (2001) Interpreting infrared, Raman, and nuclear magnetic resonance spectra, vol 2
25. Wang F, Lai Y-H, Kocherginsky NM, Kosteski YY (2003) Org Lett 5:995
26. Wang F, Lai Y-H, Han M-Y (2004) Macromolecules 37:3222
27. Ferreira CA, Domenech SC, Lacaze PC (2001) J Appl Electrochem 31:49
28. Zagórska M, Proń A, Lefrant S (1997) In: Nalwa HS (ed) Handbook of organic conductive molecules and polymers, vol 3. John Wiley & Sons, Chichester

29. Castiglioni C, Mapelli C, Negri F, Zerbi G (2001) J Chem Phys 114:963
30. Rigolio M, Castiglioni C, Zerbi G, Negri F (2001) J Mol Struct 563–564:79
31. Österholm A, Meana Esteban B, Kvarnström C, Ivaska A (2008) J Phys Chem B 112:6331
32. Swamy V, Kuznetsov A, Dubrovinsky LS, Caruso RA, Shchukin DG, Muddle BC (2005) Phys Rev B 71:184302
33. Baia L, Peter A, Cosoveanu V, Indrea E, Baia M, Popp J, Danciu V (2006) Thin Solid Films 511–512:512